

Ethanol Conversion Catalyzed by MCM-22 and Its Dealuminated and Delaminated Forms

Zilacleide S. B. Sousa,^{†a,b} Cristiane A. Henriques^{†*,a,b} and Victor T. da Silva^{†,b}

^aInstituto de Química, Universidade do Estado do Rio de Janeiro (UERJ),
Rua São Francisco Xavier, 524, Maracanã, 20550-900 Rio de Janeiro-RJ, Brazil

^bNUCAT-Programa de Engenharia Química, Universidade Federal do Rio de Janeiro,
COPPE, P.O. Box 68502, 21941-914 Rio de Janeiro-RJ, Brazil

The conversion of ethanol into hydrocarbons, particularly into light olefins, was studied over MCM-22 zeolite in their acid form (HMCM-22) and its derived forms obtained by dealumination with oxalic acid (HMCM-22(OA)) and delamination (HITQ-2). The treatment with oxalic acid did not affect zeolite textural properties but reduced the total density and strength of the acid sites. As to the delamination process, HITQ-2 zeolite presented the highest Brunauer, Emmett and Teller (BET) specific area, mesopore volume, and external area, but the microporosity was not affected. This sample showed a lower SiO₂/Al₂O₃ ratio than the precursor HMCM-22, resulting in the highest acid site density but with the predominance of acid sites with weak and intermediate strength. Both dealumination and delamination led to an increase in the number of structural defects in the samples. The comparison of the catalytic performance at 500 °C showed that despite the differences in the acidic and textural properties of the samples, they were active for ethanol conversion and highly selective for ethylene production. Ethanol conversion, followed by *in situ* diffuse reflectance spectroscopy (DRIFTS), was also investigated. It showed that, for both samples, the “coke band” intensity was already significant after 1 min of reaction, similar to what was detected for HMCM-22.

Keywords: ethanol conversion, MCM-22, ethylene, DRIFTS *in situ*, coke, ITQ-2

Introduction

The chemical industry has a growing interest in sustainable technologies from economic, environmental, and social perspectives, with an emphasis on using renewable feedstocks to produce intermediate and valuable chemicals.

In this context, many processes employing ethanol (as feedstock) have been proposed to produce different chemical compounds.¹⁻⁶ The focus on ethanol is associated with its plentiful availability and the projection that the supply of this alcohol will be even greater due to the production not only from sucrose and starch but also (and especially) from cellulosic wastes. Thus, replacing methanol of fossil origin with ethanol to produce hydrocarbons (shift from Methanol to Olefins (MTH) to Ethanol to Hydrocarbons (ETH) processes) has attracted the attention of many companies and research groups.

Different authors have reported the studies of ethanol transformation into hydrocarbons over HZSM-5 zeolites.⁷⁻¹⁰ The product distribution and the activity are influenced by the density and/or the strength of the Brønsted acid sites. HZSM-5 zeolite exhibits acidic characteristics and a porous structure that directly transforms ethanol into ethylene and C3-C8 hydrocarbons. The strong Brønsted acid sites are essential to increase the selectivity to higher hydrocarbons but not for ethylene formation.¹¹ According to Song *et al.*¹² moderate strength sites in major quantity would favor the high selectivity to propylene.

One of the routes generally accepted for ethanol conversion into ethylene is related to the dehydration of ethanol to ethyl ether for then the dehydration of the latter to ethylene,¹³ subsequently ethylene undergoes successive reactions, forming higher hydrocarbons. At low temperatures, the exclusive formation of ethyl ether by intermolecular dehydration between two ethanol molecules is observed. On the other hand, because of the thermodynamic instability of ethyl ether,¹⁴ higher

*e-mail: cah@uerj.br

[†]In memory of our colleague Victor Teixeira da Silva
Editor handled this article: Jaísa Fernandes Soares

reaction temperatures favor ethylene formation due to the intramolecular dehydration of ethanol or ethyl ether. Besides, the ethyl ether can also be transformed into C4 olefin by dehydration. Subsequently, ethylene and C4 olefins can form higher olefins, paraffins, and aromatics (benzene, toluene, xylene),¹¹ although of reactions such as oligomerization, aromatization, hydride transfer, or cracking. At temperatures below 300 °C, ethylene is the predominant primary product of ethanol conversion into hydrocarbons, and at higher temperatures, ethylene is the intermediate for the formation of olefins C3+ and aromatics.¹⁵⁻¹⁸

Understanding the reaction route is crucial for reaching a good product yield. The first step for ethanol conversion into hydrocarbons is ethanol dehydration into ethylene. According to the literature, the mechanism for the transformation of ethanol or ethylene into hydrocarbons is not yet established, and the proposal of reaction mechanisms are the carbene mechanism,¹⁹⁻²² the radical-assisted mechanism,^{23,24} the hydrocarbon pool,^{12,25-29} and the carbenium mechanism.³⁰⁻³³

Fernandes *et al.*³⁴ showed that propylene formation from ethylene occurred through one carbene species produced by two ethylene molecules. At the same time, olefins C3+ were formed by the dimerization of C₂= and C₃= and reactions involving propylene and ethylene and between butene and ethylene. Depending on the reaction temperature, different mechanisms were observed for forming aromatics and paraffins. The first one is the dehydrocyclization of C6+ olefins that liberate hydrogen in the reaction medium, forming paraffinic compounds by hydrogenation. The second is hydrogen transfer between naphthenic and olefins, generating aromatic compounds and paraffins. According to the authors, ethylene conversion and product yield changed at higher temperatures, favoring dehydrocyclization reactions. On the condition studied, the authors observed that the deactivation was associated with coke formation that influences the strongest acid sites active for cyclization, hydrogen transfer, and aromatic condensation reactions.

Lin *et al.*²⁶ studied the nature of the reaction intermediates using Fourier transform infrared (FTIR) to propose the mechanism of propylene production from ethylene. According to this study, ethylene strongly adsorbs on Brønsted acid sites and weakly on silanol groups even after 1 min of interaction. Through the IR technique, they observed that bands related to methyl and methylene groups were identified and associated with the ethylene oligomerization. After the evacuation at 300 °C, the oligomeric species remains adsorbed even and gradually form neutral or cationic oligomeric polyenic species. The explanation, second the authors, is that the cracking of the adsorbed oligomers takes the formation of propylene.

Our previous study³⁵ compared the product distribution for ethanol conversion over HZSM-5 and HMCM-22 zeolites. It was observed that the formation of propylene, butenes, paraffines (C₂-C₄), and aromatics was favored on HZSM-5. At the same time, HMCM-22 was highly selective to ethylene. The differences in their acidic, textural, and structural properties were taken into account to justify the differences observed in the distribution of the reaction products.

As to the acidic properties, since the density of acid sites, especially those with intermediate strength, is an important property to propylene selectivity¹² but not for the production of ethylene,¹¹ the formation of these two olefins could be associated with acid characteristics of these two zeolites (ZSM-5 and MCM-22).

Concerning the porous structure, both HZSM-5 and HMCM-22 are medium pores zeolites but quite different pore systems. While HZSM-5 is formed by two interconnected channel systems with similar diameters, HMCM-22 has two independent channel systems, both accessible by 10-membered (MR) ring openings with slightly smaller dimensions than those of HZSM-5. Besides this, one of the channel systems of HMCM-22 is two-dimensional, formed by sinuous channels. The other system consists of large cavities defined by 12-MR rings with an internal height of 18.2 Å and interconnected by openings formed by 10-MR rings. Moreover, in HMCM-22, the surface acid sites are located in pockets defined by 12-MR rings. We initially expected that acid sites in larger spaces than those found in HZSM-5 favor oligomerization, cyclization, and hydrogen transfer reactions, contributing to increasing olefins and aromatics selectivity. However, this behavior was not observed, and zeolite HMCM-22 was highly selective to ethylene.

Thus, continuing our previous study, the present work focused on the study of ethanol transformation into light olefins catalyzed by HMCM-22 and its derived forms produced by dealumination with oxalic acid (HMCM-22(OA)) and by delamination (HITQ-2). HITQ-2 does not have the channel system formed by the large cavities observed on HMCM-22,^{36,37} thus allowing the investigation of the effect of the acid sites location on the product formation. In addition, dealumination should modify the acidic properties of HMCM-22, putting some insights into its influence on catalytic performance. Another important aspect contemplated in the present work was the study of ethanol conversion into hydrocarbons using the *in situ* diffuse reflectance spectroscopy (DRIFTS), which was carried out to study the nature of the species formed on the zeolites along with the reaction and the role played by the acidic properties (density, strength, and location) on their formation.

Experimental

Catalysts

The HMCM-22 zeolite was synthesized accordingly to Corma *et al.*³⁸ Hexamethyleneimine (HMI) was used as the structure directing agent (SDA) (Sigma-Aldrich, Barueri, Brazil). The synthesis gel was prepared with a molar composition equal to 2.7 Na₂O:Al₂O₃:30 SiO₂:1347 H₂O:15 HMI. It was crystallized in Teflon-lined autoclaves for 7 days in an oven at 150 °C, rotating at 60 rpm and under autogenous pressure. Then, the obtained solid was filtered and washed with distilled and deionized water until the pH was lower than 7. This solid was named MCM-22(P). Part of the solid was dried at 120 °C overnight, and then the SDA was removed by thermal treatment at 550 °C for 1 h under N₂ (50 mL min⁻¹) and 9 h under dry air (50 mL min⁻¹) at the same temperature (Air Products, Mogi das Cruzes, Brazil). The obtained solid was named HMCM-22.

For the synthesis of HITQ-2, the procedure described elsewhere³⁷ was used. First, the other part of the solid MCM-22(P) was washed with distilled water up to a pH lower than 9. Then, the solid was swelled by refluxing for 16 h at 80 °C of the suspension resulting from the mixture of 5.0 g of MCM-22(P) with 100 g of hexadecyl trimethylammonium bromide solution (29 wt.%) and 30 g of tetrapropylammonium hydroxide (40 wt.%) (Sigma-Aldrich, Barueri, Brazil). Next, the layers were stripped apart in an ultrasound bath for 1 h. At this stage, the pH of the slurry approached 12.5. Subsequently, the solid phase was separated by adding drops of concentrated HCl to ensure the pH was slightly below 2. The solid was then washed with distilled water and dried at 120 °C overnight. The organic material was then removed by calcination at 540 °C for 4 h under N₂ (50 mL min⁻¹) and 8 h under dry air (50 mL min⁻¹) at the same temperature (99.995% Air Products, Mogi das Cruzes, Brazil). The obtained solid was named HITQ-2.

Dealumination was done by refluxing 10 g of HMCM-22 zeolite in 200 mL of oxalic acid solution (0.5 mol L⁻¹) for 24 h (Sigma-Aldrich, Barueri, Brazil).³⁹ After drying at 120 °C overnight, the product was calcinated under dry air (50 mL) (99.995% Air Products, Mogi das Cruzes, Brazil) at 550 °C for 4 h. The dealuminated HMCM-22 sample was named HMCM-22(OA).

Characterization

X-ray diffractograms (XRD) were acquired employing a Rigaku diffractometer (Tokyo, Japan), model Miniflex II operated at 30 kV and 15 mA, using the K α copper

radiation. The data were carried out with intervals of 0.02° and an acquisition time of 2 s from 4.0 to 60° (2 θ). The chemical composition was obtained by X-ray fluorescence (XRF) using a Rigaku spectrometer (model RIX 3100) (Tokyo, Japan), while solid-state ²⁷Al magic angle spinning nuclear magnetic resonance (MAS/NMR) determined the framework composition. The equipment used for ²⁷Al MAS/NMR analyses was a Bruker AVANCE-400 NMR spectrometer (Rheinstetten, Germany), at 9.4 T, equipped with a VT-CP/MAS 7.0 mm probe. The ²⁷Al MAS/NMR spectra were acquired at 103.9 MHz with a magic angle spinning speed of 12 kHz using 1.0 μ s ($\pi/20$) pulses and 0.5 s delay, a total of 5000 pulses being accumulated.

The Brunauer, Emmett and Teller (BET) specific area, external area and micropore volume (t-plot), and mesopore volume (Barrett-Joyner-Halenda (BJH)) of the zeolites were determined by N₂ adsorption/desorption at -196 °C in a Micromeritics ASAP 2020 instrument (Norcross, United States).

Temperature-programmed desorption (TPD) of ammonia (NH₃) was obtained from a homemade TPD/TPR/TPO dynamic device equipped with a thermal conductivity detector (TCD) (Rio de Janeiro, Brazil). First, 0.2 g of the sample was treated *in situ* at 150 °C for 1 h. Subsequently, the temperature was increased at 500 °C for 1 h under a flow of He (30 mL min⁻¹) (2.91% vol., Air Products, Mogi das Cruzes, Brazil), using a heating rate was 2 °C min⁻¹. And then, the zeolite was cooled down to 150 °C for that NH₃ adsorption under a flow of 2.91% (vol) NH₃/He (30 mL min⁻¹) (Air Products, Mogi das Cruzes, Brazil). The next step consisted of physisorbed molecules remotion under He (30 mL min⁻¹) (99.995%, Air Products, Mogi das Cruzes, Brazil) at the same temperature (150 °C), and then desorption of chemisorbed NH₃ was obtained from 150 to 500 °C using He (30 mL min⁻¹), and a rate of 10 °C min⁻¹. The total acidity was related to the ammonia chemically adsorbed at 150 °C, subtracting the physisorbed amount from the total amount of NH₃ adsorbed by the samples studied.

In situ diffuse reflectance infrared Fourier transform spectroscopy (DRIFTS)-pyridine

The DRIFTS of adsorbed pyridine is a valuable tool to identify the Brønsted and Lewis acid sites in the samples. The equipment used was PerkinElmer Spectrum 100 spectrometer with an MCT-A detector and a high-temperature chamber (Harrick) with CaF₂ windows (Waltham, United States). The spectra were obtained with a resolution of 4 cm⁻¹ and 60 scans. First, the zeolite was pretreated under a vacuum and heated from room temperature to 500 °C for 1 h, using a heating

rate of 5 °C min⁻¹. Subsequently, the sample was cooled to 150 °C, and pyridine (99.8%, Sigma-Aldrich, Barueri, Brazil) was fed into the chamber for 1 min using a He flow (30 mL min⁻¹) (99.995%, Air Products, Mogi das Cruzes, Brazil) passing through the saturator maintained at a temperature of 0 °C. Next, the sample was treated under vacuum at 150 °C for 1 h to remove the excess pyridine, and then the first spectrum was acquired. After that, the chamber temperature was raised to 250 °C under vacuum, and, after remaining at this temperature for 1 h, a new spectrum was acquired. Finally, the temperature was raised to 350 °C for 1 h under vacuum, and a new spectrum was acquired.

In situ diffuse reflectance infrared Fourier transform spectroscopy (DRIFTS)-ethanol

The evaluation of the species formed on the surface of the zeolites was realized during the reaction, *in situ* DRIFTS analyses. The equipment utilized was PerkinElmer Spectrum 100 spectrometer with an MCT-A detector and a high-temperature chamber (Harrick) with ZnSe windows (Waltham, United States). Spectra were obtained from a resolution of 4 cm⁻¹ and 150 scans. The zeolite was pretreated under He flow (30 mL min⁻¹) (99.99%, Air Products, Mogi das Cruzes, Brazil) from room temperature to 500 °C at a heating rate of 5 °C min⁻¹.

The analyses procedure involved introducing a stream of saturated ethanol/He into the chamber kept at 500 °C, and the spectra were obtained at different times (1, 5, 15, 30, and 60 min). The spectra of the pretreated samples were used as background.

Catalytic evaluation

The reaction of conversion ethanol (99.5, Sigma-Aldrich, Barueri, Brazil) was carried out at 500 °C under atmospheric pressure in a fixed bed glass micro-reactor fitted with an online gas chromatograph (capillary column HP-Plot/Q of 30 m and flame ionization detector). The gas feed containing ethanol vapor was obtained by N₂ stream (50 mL min⁻¹) passed through a saturator maintained at 32 °C and then sent to the reactor containing the catalyst. The partial pressure of ethanol was 0.12 atm,

and the space velocity was 6.5 g_{EtOH} g_{cat}⁻¹ h⁻¹. Before the reaction, the zeolites were thermally treated *in situ* from room temperature up to 500 °C in flow N₂ (50 mL min⁻¹) (99.995%, Air Products, Mogi das Cruzes, Brazil) at a heating rate of 2 °C min⁻¹ and kept at this temperature for 1 h for the elimination of water and other adsorbed species.

Results and Discussion

Chemical composition

Table 1 presents the bulk and framework chemical composition of zeolites. Our previous study³⁵ showed that the preparation method for HMCM-22 was efficient since the Si/Al ratio obtained was close to the nominal value of 30. Sodium was not detected in any of the samples. The bulk and framework chemical analysis results for sample HITQ-2 (Table 1) showed that the SAR (SiO₂/Al₂O₃ molar ratio) of this material is lower than that of the precursor HMCM-22. This reduction of the SAR value can be associated with the intercalation step (swelling) occurring in a strongly alkaline medium, which promotes the preferential leaching of the silicon species from the zeolite, originating a delaminated material with lower SAR than the precursor.³⁸ As to the dealumination with oxalic acid, the process increased the global SAR from 27 (original sample) to 36.

For the studied zeolites, the framework SAR obtained by ²⁷Al MAS/NMR was higher than those obtained by XRF, indicating the presence of extra-framework aluminum species (EFAL). In the case of zeolite HMCM-22(OA), this effect was more significant. The increase of framework SAR may be related to the calcination of zeolites to eliminate the template, causing framework dealumination and generating EFAL species, as reported in the literature by different authors.³⁹⁻⁴²

X-ray diffractometry

The X-ray diffractograms of the samples are presented in Figure 1. The comparison with the standard diffractograms reported in the literature shows that the HMCM-22 is pure and highly crystalline.^{35,39}

Table 1. Bulk and framework chemical composition of zeolites

| Sample | Na ₂ O / % | SiO ₂ / % | Al ₂ O ₃ / % | Bulk SAR ^a | Framework SAR ^b |
|----------|-----------------------|----------------------|------------------------------------|-----------------------|----------------------------|
| HMCM-22 | 0 | 94.0 | 6.0 | 27 | 35 |
| HMCM(OA) | 0 | 95.5 | 4.5 | 36 | 48 |
| HITQ-2 | 0 | 93.2 | 6.8 | 23 | 28 |

^aXRF: X-ray fluorescence spectroscopy; ^b²⁷Al MAS magic angle-spinning; NMR: nuclear magnetic resonance spectrum. SAR: SiO₂/Al₂O₃ molar ratio,

The formation of the zeolite HITQ-2, which has a less ordered structure than HMCM-22,^{36,37} was demonstrated by the X-ray diffractogram presented in Figure 1d, which shows the presence of broader and low-intensity peaks, indicating a partially amorphous disordered structure. As observed by scanning electron microscopy (SEM) (not shown), HITQ-2 is formed by thin layers in a disordered arrangement, while for HMCM-22, the layers were well-ordered. The small particle size also contributed to broadening the peaks in the diffractogram.

X-ray diffraction patterns indicate that dealumination did not affect the zeolite structure since the diffractograms of the original and dealuminated zeolite were virtually identical, without additional crystalline phases (Figures 1b, 1c). Nevertheless, there was a slight increase in the peaks' intensity. The crystallinity value for HMCM-22(OA), based on the intensities of the 2 θ peaks (22.45 to 28.5°) and utilizing the parent sample as standard, was 109%. As suggested by Cambor *et al.*⁴³ and Mihályi *et al.*,⁴⁴ the increase in the intensity of diffraction peaks can be associated with the removal of the aluminum species from the framework, resulting in a more ordered crystalline structure.

Textural analysis

The N₂ physisorption isotherms of the zeolites are shown in Figure 2 (HMCM-22, HMCM-22(OA), HITQ-2), while Table 2 reports their textural properties.

Figure 2 compares the N₂ physisorption isotherms of the studied samples. HMCM-22 and HMCM-22(OA) have a type I isotherm typical of microporous solids. The asymptotic increase in the adsorbed volume observed for $p/p_0 \rightarrow 1$ could be associated with the filling of intercrystalline space with the adsorbate. On the other hand, HITQ-2 shows type IV isotherm with a hysteresis loop starting at p/p_0 close to 0.6, and a substantial increase in the N₂ adsorbed volume as the relative pressure increases, reflecting the presence of mesopores and the growth of the external area resulting from the delamination. As shown in Table 2, HITQ-2 presented the highest BET specific area, mesopore volume, and external area, which can also be associated with its

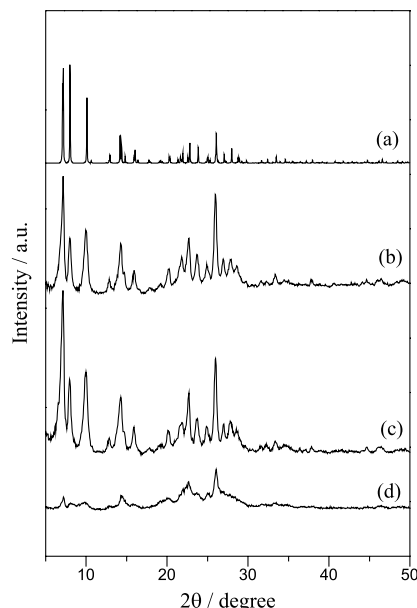


Figure 1. X-ray diffractograms for (a) framework type MWW standard, (b) HMCM-22, (c) HMCM-22(OA), and (d) HITQ-2.

partially disordered structure. Corma *et al.*³⁶ observed that the delamination decreases the micropore volume and increases the external surface area compared to the precursor sample. In addition, the delamination results in the disappearance of large cavities and the replacement by external “cups”, while the 10-MR circular channel still exists in the material. In this work, it was observed an increase in external surface area, although on a lower scale than those reported in the literature.^{36,45} Moreover, the microporosity was quite similar to the HMCM-22 precursor. These results suggest that the delamination was incomplete.

Table 2 also shows that the treatment of HMCM-22 with oxalic acid did not affect the textural properties of the zeolite.

Temperature programmed desorption of ammonia-NH₃ TPD

The total density of acid sites and the distribution of their strength were obtained by temperature programmed desorption of ammonia (NH₃-TPD). The total density of acid sites, corresponding to the chemically adsorbed

Table 2. Textural properties of zeolites

| Zeolite | $S_{\text{BET}} / (\text{m}^2 \text{g}^{-1})$ | $S_{\text{Ext}} / (\text{m}^2 \text{g}^{-1})$ | $V_{\text{Mic}} / (\text{cm}^3 \text{g}^{-1})$ | $V_{\text{Mes}} / (\text{cm}^3 \text{g}^{-1})$ |
|--------------|---|---|--|--|
| HMCM-22 | 509 | 80 | 0.20 | 0.36 |
| HMCM-22 (OA) | 493 | 86 | 0.19 | 0.37 |
| HITQ-2 | 633 | 246 | 0.19 | 0.82 |

S_{BET} : Brunauer-Emmett-Teller surface area; S_{Ext} : t-plot external surface area; V_{mic} : t-Plot micropore volume; V_{mes} : BJH (Barrett, Joyner, and Halenda) adsorption cumulative volume of pores (17 to 3000 Å).

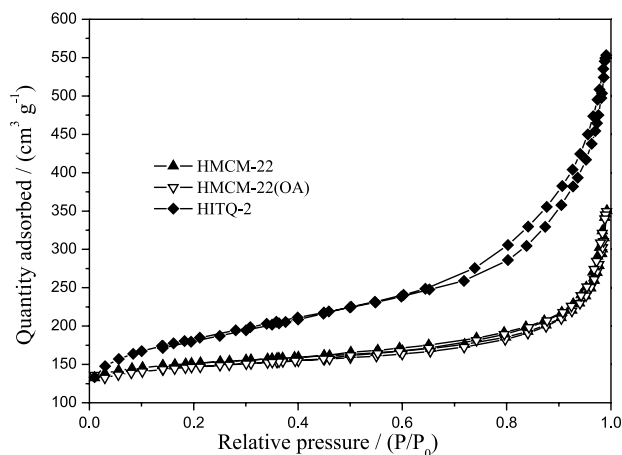


Figure 2. N₂ adsorption and desorption isotherms of the studied samples.

ammonia, is presented in Table 3, together with the concentrations of the weak, intermediate, and strong acid sites. These were obtained by decomposition of the profiles (Figures S3, S4, and S5, Supplementary Information (SI) section) into three peaks, the first one corresponding to desorption at temperatures lower than 290 °C, associated with weak sites; the second corresponding to the ammonia desorbed at temperatures between 290 and 350 °C, related to the intermediate sites; and the third corresponding to the desorption at temperatures higher than 350 °C, related to the strong acid sites. Table 3 also shows the maximum desorption temperatures of NH₃ associated with the three types of sites, which represents their acid strength.

The following sequence was observed concerning the total acid site density: HITQ-2 > HMCM-22 > HMCM-22(OA), which followed the same order observed for the framework aluminum content. The results presented in Table 3 indicated that the dealumination of HMCM-22 with oxalic acid reduced not only the total density of the acid sites but also the strength of the acid sites since the maximum desorption temperatures are shifted to lower values for HMCM-22(OA). Moreover, the relative amount of strong acid sites is lower for HMCM-22(OA) than for HMCM-22, suggesting the preferential removal of the aluminum atoms associated with the weak and intermediate acid sites by dealumination. Ren *et al.*⁴⁶ also characterized the acidity of samples of HMCM-22 dealuminated by oxalic

acid employing temperature programmed desorption of ammonia. They observed a drop in the acid site density and a decline in the acid sites' strength.

As for HITQ-2, which has the highest acid site density, the predominance of weak and intermediate strength acid sites was observed.

Diffuse reflectance infrared Fourier transform spectroscopy (DRIFTS) with pyridine adsorption

The vibration of the hydroxyl groups present on the surface of the zeolites can be observed by infrared spectroscopy between 3800-3400 cm⁻¹. Comparing the spectra obtained before and after pyridine adsorption allows identifying, among the different types of hydroxyl groups, those with acidic character.

Figure 3 shows the infrared spectra in the region of the hydroxyl groups for the samples HMCM-22, HMCM-22(OA), and HITQ-2. Spectrum (Figure 3a) was obtained after thermal treatment under vacuum at 500 °C and spectrum (Figure 3b) after pyridine adsorption at 150 °C, followed by thermal treatment under vacuum at the same temperature. Spectrum (Figure 3c) corresponds to the difference between spectra (Figures 3a and 3b) and shows the bands associated with the hydroxyls with acid character.

Figure 3 shows that the band at 3600 cm⁻¹ is associated with the Brønsted acid sites (bridging OH groups Si(OH)Al), while those at 3743 cm⁻¹ are related to the hydroxyls of the silanol groups.

All zeolites present a band at 3660 cm⁻¹, associated with the presence of EFAL species. Furthermore, a small fraction of these species showed acid character, revealed by the shoulder at 3660 cm⁻¹ for all samples in the spectrum (Figure 3c). According to Corma *et al.*,³⁹ the thermal treatment of MCM-22 zeolites to remove organic templates can partially dealuminate them, generating extra-framework aluminum, whose presence can be verified by the band around 3670 cm⁻¹. Min *et al.*⁴⁵ also observed the presence of EFAL due to the treatment of the MCM-22 precursor to generate the acid form.

HMCM-22 and HITQ-2 present a band associated with the silanol groups (3743 cm⁻¹), indicating structural

Table 3. Total acidity and acid strength distribution

| Zeolite | Total acidity | | Weak | | Moderate | | Strong | |
|------------|---|-----------------------|---|-----------------------|---|-----------------------|---|--|
| | Concentration of acid sites / (μmol NH ₃ g ⁻¹) | T _{max} / °C | Concentration of acid sites / (μmol NH ₃ g ⁻¹) | T _{max} / °C | Concentration of acid sites / (μmol NH ₃ g ⁻¹) | T _{max} / °C | Concentration of acid sites / (μmol NH ₃ g ⁻¹) | |
| HMCM-22 | 938 | 283 | 225 | 323 | 169 | 452 | 544 | |
| HMCM-2(OA) | 734 | 259 | 133 | 305 | 92 | 439 | 509 | |
| HITQ-2 | 1102 | 268 | 474 | 329 | 264 | 420 | 364 | |

T_{max}: maximum temperature.

defects. The presence of this band can be related to the calcination process to remove the template.³⁹ Part of the hydroxyls of the silanol groups in HMCM-22 and HITQ-2 had an acidic character, suggesting that the rest of the hydroxyls are neutral or, in the case of HMCM-22, are located in positions inaccessible to the pyridine molecules. According to Corma and co-workers⁴⁷ silanol groups are present on the internal surface (inside the 10-MR channels) and external surface (located in the pockets) of the MCM-22 crystal. Furthermore, the spectrum of HMCM-22 also had a shoulder at 3727 cm⁻¹, which is associated with the presence of hydroxy nests in the structure of the zeolite MCM-22.⁴⁴

The spectrum in Figure 3Ba for HMCM-22(OA) contains a band associated with silanol groups at 3743 cm⁻¹, which is slightly more intense than that present in the spectra of the precursor, indicating that the dealumination led to an increase in the number of structural defects present in the sample. The band at 3660 cm⁻¹ (Figure 3Bc) indicates that the dealumination process with oxalic acid generated EFAL and did not leach the extra-framework aluminum species originally present. Comparison of the spectra (Figure 3Ba) of HMCM-22(OA) and HMCM-22 indicates a slight decrease in the Brønsted acid sites' intensity for sample HMCM-22(OA), thus reflecting a reduction in the number of acid sites with the decrease in the framework aluminum due to the dealumination (increase in the framework SAR, Table 1). A similar trend was observed from NH₃ TPD.

Figure 4 presents the infrared spectra, in the range from 1700 to 1400 cm⁻¹, for the samples HMCM-22, HMCM-22(OA), and HITQ-2 related to the pyridine

that remained adsorbed after the thermal treatment under vacuum at 150 °C (a), 250 °C (b), and 350 °C (c).

For all the studied samples, bands are observed at 1547 cm⁻¹, corresponding to the pyridine adsorbed in Brønsted acid sites (as pyridinium ions); at 1457 cm⁻¹, corresponding to the pyridine coordinated with the Lewis acid sites; and at 1490 cm⁻¹, corresponding to the adsorption in both Brønsted and Lewis sites. These results agree with those reported in the literature for zeolite HMCM-22.⁴⁷⁻⁴⁹ Other bands were identified at 1637 cm⁻¹, attributed to the pyridine ions formed in the Brønsted acid sites, and at 1625 cm⁻¹, associated with the Lewis acid sites.⁴⁹ The pyridine adsorption spectra of the zeolites (Figure 4) indicate the predominance of Brønsted acid sites. Many of these sites have sufficient acid strength to keep the pyridine adsorbed up to 350 °C. The dealuminated samples showed a slight increase in the intensity of the band associated with the Lewis acid sites.

Catalytic evaluation

The catalytic performance of the zeolites (HMCM-22, HMCM-22(OA), and HITQ-2) was compared under experimental conditions selected from our previous study using HZSM-5.¹⁸ These conditions were the most favorable to the formation of propylene from ethanol (500 °C, weight hourly space velocity (WHSV) of 6.5 g_{EiOH} g_{cat.}⁻¹ h⁻¹, ethanol partial pressure of 0.12 atm, and reaction time of 4.5 h (270 min)).

The product distribution (molar%) for the zeolites at the beginning of the reaction (10 min) and after 270 min

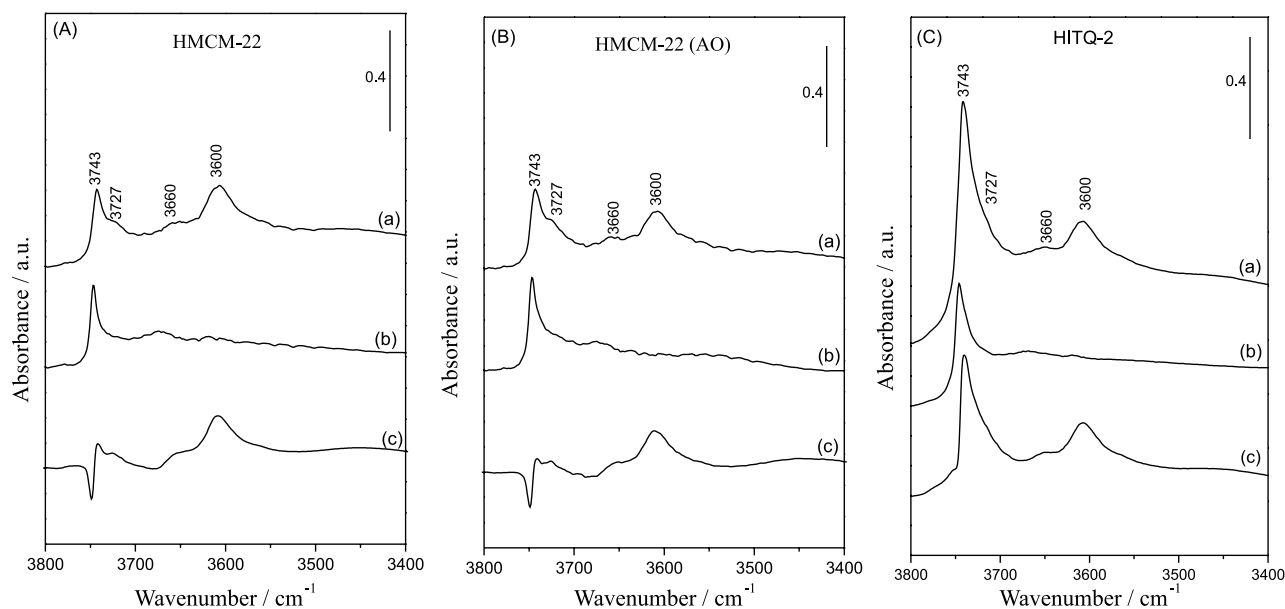


Figure 3. DRIFTS spectra of the studied zeolites: (a) after treatment at 500 °C under vacuum; (b) after adsorption of pyridine and desorption at 150 °C (c) difference between spectra (a) and (b).

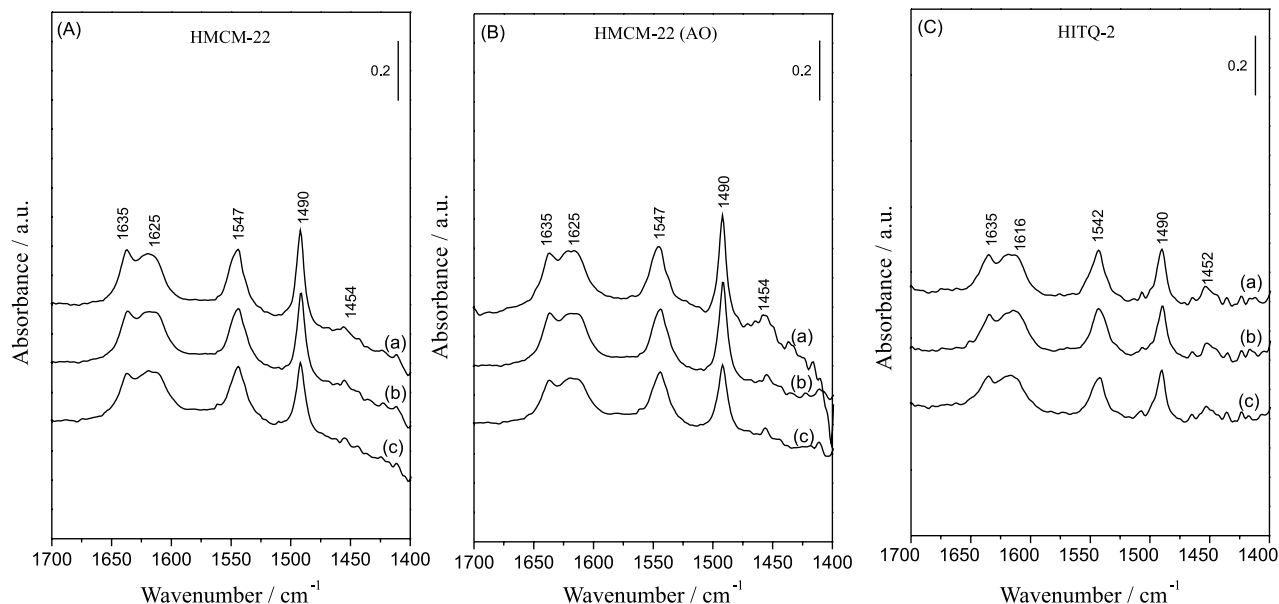


Figure 4. DRIFTS spectra of the studied zeolites: (a) after adsorption of pyridine and desorption at 150 °C, (b) after desorption at 250 °C, and (c) after desorption at 350 °C.

(4.5 h) is compared in Table 4. Under the studied conditions, ethanol conversion was 100% along the reaction, and ethyl ether was not detected among the products. The time-on-stream (TOS) did not significantly influence ethanol conversion and product distribution. Moreover, the differences in the acidic properties and porous structures of the studied zeolites did not affect the product distribution since ethylene was virtually the unique product formed for all samples.

According to the literature,^{44,46,50,51} dealumination of HMCM-22 with oxalic acid should preferentially affect the surface acid sites in the external pockets. Thus, the acid sites in the large cavities and sinuous channels should predominate in HMCM-22(OA). The dealumination with OA did not substantially affect the textural properties (Table 2) but reduced the total density of acid sites and their acid strength distribution (Table 3).

The characterization of the coke deposited in the zeolite HMCM-22 after 4.5 h and the *in situ* DRIFTS monitoring of the reaction were discussed in detail by Sousa *et al.*,³⁵ and show that the voluminous compounds, such as olefins, paraffins, and aromatics, are generated after short reaction times and are retained inside the porous structure of HMCM-22. Comparing this zeolite with HZSM-5 showed that coke formation is more significant in HMCM-22 since the HZSM-5 porous structure restricts the formation of voluminous molecules. As a result, the simple aromatic compounds formed diffuse through the three-dimensional porous structure of HZSM-5 and are detected as products. However, the low selectivity to C₃+ hydrocarbons and the more significant amount of coke observed for HMCM-22

Table 4. Product distribution for HMCM-22, HMCM-22(OA) and HITQ-2 zeolites after TOS = 10 min and TOS = 270 min ($X_{\text{EtOH}} = 100\%$, $\text{WHSV} = 6.5 \text{ g}_{\text{EtOH}} \text{ g}_{\text{cat}}^{-1} \text{ h}^{-1}$, $T = 500 \text{ }^\circ\text{C}$, $p_{\text{EtOH}} = 0.12 \text{ atm}$)

| | time / min | Product distribution (molar) / % | | |
|---|------------|----------------------------------|--------------|--------|
| | | HMCM-22 | HMCM-22 (OA) | HITQ-2 |
| C ₁ | 10 | 0.1 | 0.1 | 0.1 |
| | 270 | 0.1 | 0.1 | 0.0 |
| C ₂ -C ₄ | 10 | 0.3 | 0.8 | 0.4 |
| | 270 | 0.1 | 0.1 | 0.1 |
| C ₂ H ₄ | 10 | 95.6 | 94.2 | 96.2 |
| | 270 | 97.5 | 97.8 | 99.0 |
| C ₃ H ₆ | 10 | 2.2 | 3.2 | 2.0 |
| | 270 | 1.0 | 1.0 | 0.4 |
| C ₄ H ₈ | 10 | 1.3 | 1.1 | 0.9 |
| | 270 | 1.0 | 0.8 | 0.5 |
| C ₅ -C ₅ ⁼ | 10 | 0.3 | 0.4 | 0.3 |
| | 270 | 0.2 | 0.1 | 0.0 |
| BTX | 10 | 0.0 | 0.1 | 0.1 |
| | 270 | 0.0 | 0.1 | 0.0 |
| C ₆ ⁺ | 10 | 0.2 | 0.1 | 0.0 |
| | 270 | 0.1 | 0.0 | 0.0 |

BTX: benzene, toluene, xylene.

indicates that the strong and intermediate acid sites, which undergo reactions of oligomerization, cyclization, aromatization, and hydride transfer, responsible for forming the heavier products, are preferentially located in the large cavities and the external pocket. The 10-MR openings of the large cavities restrict the diffusion of the products outside

the pores, so they remain retained inside the structure as coke. Moreover, the rapid formation of coke blocks the active sites at the external pockets. Both facts could explain the reduced production of C₃+ hydrocarbons observed since the beginning of the reaction.

Since the conversion of ethanol to ethylene occurred even in weak acid sites, the high selectivity to ethylene over HMCM-22 suggests that weak acid sites predominated in the sinuous porous system of HMCM-22. Thus, ethylene would be formed preferentially in the sinuous channels where the steric restrictions to forming more voluminous products (coke) kept the zeolite active and selective to ethylene even after deactivation of the sites located in other points of the porous structure.

The results obtained for HMCM-22(OA) are similar to those observed for HMCM-22. The high selectivity to ethylene is associated with the formation of this olefin in the weak acid sites that are predominant in the sinuous channels, where steric impediments restrict the production of more voluminous products. HMCM-22(OA) also contains large cavities, where strong and moderate sites promote the reactions of oligomerization, cyclization, aromatization, and hydride transfer, responsible for forming C₃+ hydrocarbons and voluminous coke molecules. The latter were retained because of the limited opening size of the large cavities (10-MR rings), thus deactivating the acid sites. The reduced formation of the C₃+ hydrocarbons along the reaction is also associated with the blockage of the sites in the external pockets by the coke molecules.

A comparison of the zeolites HMCM-22 and HITQ-2 (Table 4) shows that the distribution of products was very similar despite the differences in their acidic and textural properties, with the delaminated zeolite being also highly selective to the formation of ethylene.

As established in the literature,⁴⁵ delamination eliminates the system of channels formed by the supercavities. Thus, the porous structure of HITQ-2 has only a system of sinuous channels (10-MR opening) and external pockets. Under the conditions studied here, the delamination increased the total density of acid sites of the zeolite, which can be related to the increase in the aluminum content (both total and framework, as shown in Table 1). However, the contribution of the acid sites on the external pockets to the total acidity of the sample cannot be despised. Furthermore, the structural disorder promoted by the delamination generated a solid with larger BET and external areas and a micropore volume equal to the values observed for HMCM-22 and HMCM-22(OA).

Therefore, as proposed for HMCM-22 and HMCM-22(OA), the high selectivity to ethylene is

associated with the reaction catalyzed by the weak acid sites present in the sinuous channels where coke formation is restricted. On the other hand, in HITQ-2, the contribution of the external pockets (predominance of strong and intermediate acid sites) is greater than in HMCM-22,³⁵ explaining the tendencies observed for the coke formation in these acid sites after short reaction times, being responsible for their deactivation.

Ethanol conversion followed *in situ* by DRIFTS

The ethanol conversion followed by DRIFTS over the zeolites HITQ-2 and HMCM-22(OA) was carried out at the same temperature used in the catalytic tests (500 °C). The results were compared with those reported for HMCM-22 in our previous work.³⁵

With the reaction chamber maintained at 500 °C, a stream of ethanol/He was fed, and the spectra were acquired after 1, 5, 15, 30, and 60 min (spectra a to e of Figures 5 and 6, respectively). The region analyzed was 3200-800 cm⁻¹ since we did not observe any significant alterations in the wavenumber range between 4000 and 3200 cm⁻¹.

HITQ-2

Analysis of the spectra Figures 5a-5e shows that the ethanol/He current contact with the sample at 500 °C generated species whose fundamental vibrations presented bands between 3200 and 2800 cm⁻¹. The band at 3130 cm⁻¹, associated with the C-H stretching of aromatic ring carbon,⁵² indicates the formation of aromatic compounds deposited on the zeolite's surface.

Bands associated with C-H olefinic carbon (3080 cm⁻¹) and those related to asymmetric and symmetric stretching of the CH₃ and CH₂ groups (2984, 2935, and 2880 cm⁻¹)⁵³⁻⁵⁶ were also observed. Particularly for reaction times equal to or higher than 15 min, the intensity of the last three bands increased. The presence of these bands, associated with methyl and methylene groups, suggests the gradual formation of coke precursors adsorbed on the surface of the zeolites.⁵⁷ It should also be considered that the presence of ethoxy species, intermediate in the reaction, adsorbed on the acid sites also might contribute to the appearance of these bands.

Analysis of Figure 5 revealed the presence of bands at 950, 1030, 1160, and 1600 cm⁻¹ since the beginning of the reaction (1 min). The latter band can be related to the C=C stretching of olefins (and/or aromatic rings) attributed to the coke precursors.^{58,59}

The same bands were identified in the DRIFTS spectra for HITQ-2 (Figure 5) and HMCM-22,³⁵ suggesting that similar carbons species were formed on the surface sites of

both zeolites. The effect of time on bands' intensity was also identical for HITQ-2 and HMCM-22 except for the band at 1600 cm^{-1} , which was intense since 1 min of reaction and did not undergo significant change with longer reaction times differently to that was observed for HMCM-22.³⁵

Considering that the porous structure of HITQ-2 is formed only by the sinuous channels and external pockets, the presence of the band at 1600 cm^{-1} with high intensity since the beginning of the reaction suggests that coke formation occurs preferentially in the strong acid sites mainly located in the external pockets. As a result, a rapid formation of coke occurred at shorter reaction times, and the active sites were quickly deactivated. On the other hand, in HMCM-22, the acid sites that catalyze coke formation were mainly in the system of channels formed by the large cavities ($7.1 \times 18.2\text{ \AA}$), where the gradual formation of coke is reflected by the gradual increase in the intensity of the band at 1600 cm^{-1} .

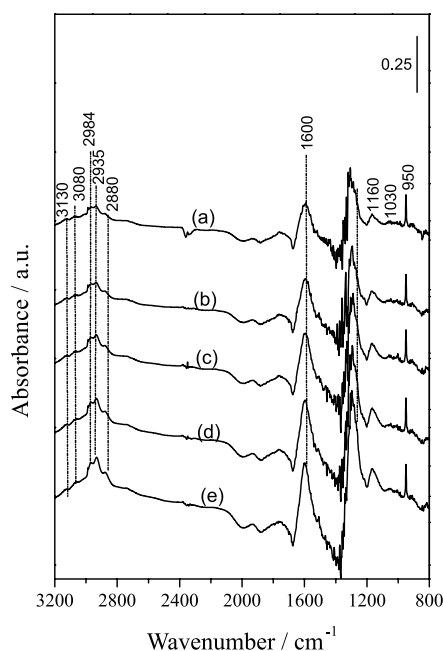


Figure 5. DRIFTS spectra of HITQ-2 zeolite obtained at $500\text{ }^{\circ}\text{C}$ under flow of ethanol/He (a) after 1 min, (b) after 5 min, (c) after 15 min, (d) after 30 min, (e) after 60 min.

HMCM-22(OA)

As for the precursor HMCM-22, the DRIFTS spectra of the dealuminated sample HMCM-22(OA) (Figure 6) showed the same bands during the studied reaction period. The difference is that the bands are slightly less intense for the dealuminated sample compared with those present in the parent sample. This behavior reflects the lower density of acid sites, revealed by the NH_3 -TPD analyses, which contributed to reducing the coking rate. However, the catalytic tests did not show evidence of this fact.

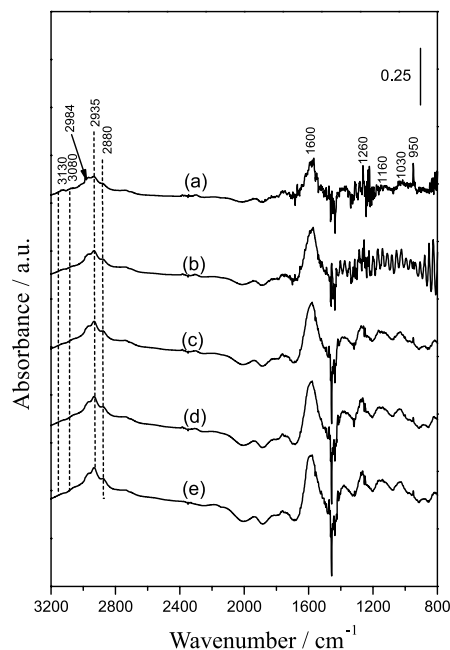


Figure 6. DRIFTS spectra of HMCM-22(OA) obtained at $500\text{ }^{\circ}\text{C}$ under flow of ethanol/He (a) after 1 min, (b) after 5 min, (c) after 15 min, (d) after 30 min, (e) after 60 min.

Conclusions

The acid form of MCM-22 zeolite (HMCM-22) and its derived forms obtained by dealumination with oxalic acid (HMCM-22(OA)) and delamination (HITQ-2) were evaluated in the conversion of ethanol into hydrocarbons.

The treatment with oxalic acid did not affect zeolite textural properties. However, it reduced the total density and strength of the acid sites, thus reflecting a partial dealumination of the zeolite (framework SAR increases from 35 to 48).

Concerning the delamination process, HITQ-2 zeolite presented the highest BET specific area, mesopore volume, and external area, but the microporosity was not affected. The increase in the external area was lower than expected for the total delamination of the precursor, which suggests that delamination was incomplete. The HITQ-2 sample showed a lower $\text{SiO}_2/\text{Al}_2\text{O}_3$ ratio than the precursor HMCM-22, resulting in the highest acid site density but with the predominance of acid sites with weak and intermediate strength. Both dealumination and delamination led to an increase in the number of structural defects in the samples.

Under the studies conditions ($T = 500\text{ }^{\circ}\text{C}$, partial pressure of ethanol = 0.12 atm ; $\text{WHSV} = 6.5\text{ g}_{\text{EtOH}}\text{ h}^{-1}\text{ g}_{\text{cat}}^{-1}$), despite the differences in the acidic and textural properties of the samples, the three zeolites were active for ethanol conversion ($X = 100\%$) and ethylene is the main product formed (selectivity $> 95\%$).

Ethanol conversion followed by *in situ* DRIFTS showed that, for all samples, the “coke band” intensity was already significant after 1 min of reaction. This fact suggests that the deposition of coke molecules from the beginning of the reaction occurs mainly on the acid sites that catalyze ethylene conversion into higher hydrocarbons. This rapid acid site deactivation was not affected by the site’s location and let active the sites that promote the conversion of ethanol into ethylene, leveling off the catalytic performance of the zeolites.

So, these results show that attempting to adjust the acidic and/or textural properties to favor the formation of valuable olefins or aromatics from ethanol is challenging in the case of the MCM-22 zeolite.

Supplementary Information

Supplementary information (^{27}Al MAS NMR spectra and NH_3 -TPD profiles of zeolites) is available free of charge at <http://jbcs.sbq.org.br> as PDF file.

Acknowledgments

The authors acknowledge Conselho Nacional de Desenvolvimento Científico e Tecnológico (CNPq) for Z. S. B. Sousa scholarship. C. A. Henriques thanks UERJ (PROCIENCIA Program), CNPq, and FAPERJ for the financial support.

References

1. Eagan, N. M.; Moore, B. M.; McClland, D. J.; Wittrig, A. M.; Canales, E.; Lanci, M. P.; Huber, G. W.; *Green Chem.* **2019**, *21*, 3300. [Crossref]
2. Zhao, Y.; Li, S.; Wang, Z.; Wang, S.; Wang, S.; Ma, X.; *Chin. Chem. Lett.* **2020**, *31*, 535. [Crossref]
3. Il Ahn, C.; Kim, C.; Bae, J. W.; Jeon, J.; Jung, H. S.; Kim, Y. B.; Lee, S.; Lee, J.; Ha, K. S.; *Fuel Process. Technol.* **2020**, *200*, 106317. [Crossref]
4. Akiyama, S.; Miyaji, A.; Hayashi, Y.; Hiza, M.; Sekiguchi, Y.; Koyama, T.-r.; Shiga, A.; Baba, T.; *J. Catal.* **2018**, *359*, 184. [Crossref]
5. Chagas, L. H.; Zonetti, P. C.; Matheus, C. R. V.; Rabello, C. R. K.; Alves, O. C.; Appel, L. G.; *ChemCatChem* **2019**, *11*, 5625. [Crossref]
6. Pang, J.; Zheng, M.; Wang, Z.; Liu, S.; Li, X.; Li, X.; Wang, J.; Zhang, T.; *Chin. J. Catal.* **2020**, *41*, 672. [Crossref]
7. Madeira, F. F.; Gnep, N. S.; Magnoux, P.; Maury, S.; Cadran, N.; *Appl. Catal., A* **2009**, *367*, 39. [Crossref]
8. Inaba, M.; Murata, K.; Takahara, I.; Inoue, K. I.; *J. Chem. Technol. Biotechnol.* **2011**, *86*, 95. [Crossref]
9. Furumoto, Y.; Harada, Y.; Tsunoji, N.; Takahashi, A.; Fujitani, T.; Ide, Y.; Sadakane, M.; Sano, T.; *Appl. Catal., A* **2011**, *399*, 262. [Crossref]
10. Xia, W.; Wang, F.; Mu, X.; Chen, K.; Takahashi, A.; Nakamura, I.; Fujitani, T.; *Catal. Commun.* **2017**, *91*, 62. [Crossref]
11. Inaba, M.; Murata, K.; Saito, M.; Takahara, I.; *React. Kinet. Catal. Lett.* **2006**, *88*, 135. [Crossref]
12. Song, Z.; Takahashi, A.; Mimura, N.; Fujitani, T.; *Catal. Lett.* **2009**, *131*, 364. [Crossref]
13. Takahara, I.; Saito, M.; Inaba, M.; Murata, K.; *Catal. Lett.* **2005**, *105*, 249. [Crossref]
14. Jingfa, D.; Guirong, Z.; Shuzhong, D.; Haishui, P.; Huaiming, W.; *Appl. Catal.* **1988**, *41*, 13. [Crossref]
15. Ghashghaee, M.; *Rev. Chem. Eng.* **2018**, *34*, 595. [Crossref]
16. Hulea, V.; *ACS Catal.* **2018**, *8*, 3263. [Crossref]
17. Li, X.; Kant, A.; He, Y.; Thakkar, H. V.; Atanga, M. A.; Rezaei, F.; Ludlow, D. K.; Rownaghi, A. A.; *Catal. Today* **2016**, *276*, 62. [Crossref]
18. Sousa, Z. S. B.; Veloso, C. O.; Henriques, C. A.; Teixeira da Silva, V.; *J. Mol. Catal. A: Chem.* **2016**, *422*, 266. [Crossref]
19. Takahashi, A.; Xia, W.; Wu, Q.; Furukawa, T.; Nakamura, I.; Shimada, H.; Fujitani, T.; *Appl. Catal., A* **2013**, *467*, 380. [Crossref]
20. Chang, C. D.; Silvestri, A. J.; *J. Catal.* **1977**, *47*, 249. [Crossref]
21. Yamazaki, H.; Shima, H.; Imai, H.; Yokoi, T.; Tatsumi, T.; Kondo, J. N.; *Angew. Chem., Int. Ed.* **2011**, *50*, 1853. [Crossref]
22. Yamazaki, H.; Shima, H.; Imai, H.; Yokoi, T.; Tatsumi, T.; Kondo, J. N.; *J. Phys. Chem. C* **2012**, *116*, 24091. [Crossref]
23. Madeira, F. F.; Gnep, N. S.; Magnoux, P.; Vezin, H.; Maury, S.; Cadran, N.; *Chem. Eng. J.* **2010**, *161*, 403. [Crossref]
24. Madeira, F. F.; Vezin, H.; Gnep, N. S.; Magnoux, P.; Maury, S.; Cadran, N.; *ACS Catal.* **2011**, *1*, 403. [Crossref]
25. Batchu, R.; Galvita, V. V.; Alexopoulos, K.; Van der Borght, K.; Poelman, H.; Reyniers, M. F.; Marin, G. B.; *Appl. Catal., A* **2017**, *538*, 207. [Crossref]
26. Lin, B.; Zhang, Q.; Wang, Y.; *Ind. Eng. Chem. Res.* **2009**, *48*, 10788. [Crossref]
27. Gayubo, A. G.; Tarrío, A. M.; Aguayo, A. T.; Olazar, M.; Bilbao, J.; *Ind. Eng. Chem. Res.* **2001**, *40*, 3467. [Crossref]
28. Johansson, R.; Hruby, S. L.; Rass-Hansen, J.; Christensen, C. H.; *Catal. Lett.* **2009**, *127*, 1. [Crossref]
29. Allotta, P. M.; Stair, P. C.; *ACS Catal.* **2012**, *2*, 2424. [Crossref]
30. Costa, E.; Uguina, A.; Aguado, J.; Hernandez, P. J.; *Ind. Eng. Chem. Process Des. Dev.* **1985**, *24*, 239. [Crossref]
31. Derouane, E. G.; Nagy, J. B.; Dejafve, P.; van Hooff, J. H. C.; Spekman, B. P.; Védrine, J. C.; Naccache, C.; *J. Catal.* **1978**, *53*, 40. [Crossref]
32. Spoto, G.; Bordiga, S.; Ricchiardi, G.; Scarano, D.; Zecchina, A.; Borello, E.; *J. Chem. Soc., Faraday Trans.* **1994**, *90*, 2827. [Crossref]

33. Bolis, V.; Védryne, J. C.; Van de Berg, J. P.; Wolthuizen, J. P.; Derouane, E. G.; *J. Chem. Soc., Faraday Trans. 1* **1980**, *76*, 1606. [Crossref]
34. Fernandes, D. S.; Veloso, C. O.; Henriques, C. A.; *Catal. Lett.* **2020**, *150*, 738. [Crossref]
35. Sousa, Z. S. B.; Cesar, D. V.; Henriques, C. A.; da Silva, V. T.; *Catal. Today* **2014**, *234*, 182. [Crossref]
36. Corma, A.; Fornes, V.; Martínez-Triguero, J.; Pergher, S. B.; *J. Catal.* **1999**, *186*, 57. [Crossref]
37. Corma, A.; Fornés, V.; Guil, J. M.; Pergher, S.; Maesen, T. L. M.; Buglass, J. G.; *Microporous Mesoporous Mater.* **2000**, *38*, 301. [Crossref]
38. Frontera, P.; Testa, F.; Aiello, R.; Candamano, S.; Nagy, J. B.; *Microporous Mesoporous Mater.* **2007**, *106*, 107. [Crossref]
39. Corma, A.; Corell, C.; Pérez-Pariente, J.; *Zeolites* **1995**, *15*, 2. [Crossref]
40. Xia, J.; Mao, D.; Tao, W.; Chen, Q.; Zhang, Y.; Tang, Y.; *Microporous Mesoporous Mater.* **2006**, *91*, 33. [Crossref]
41. Marques, A. L. S.; Monteiro, J. L. F.; Pastore, H. O.; *Microporous Mesoporous Mater.* **1999**, *32*, 131. [Crossref]
42. Lawton, S. L.; Fung, A. S.; Kennedy, G. J.; Alemany, L. B.; Chang, C. D.; Hatzikos, G. H.; Lissy, D. N.; Rubin, M. K.; Timken, H.-K. C.; Steuernagel, S.; Woessner, D. E.; *J. Phys. Chem.* **1996**, *100*, 3788. [Crossref]
43. Cambor, M. A.; Corma, A.; Diaz-Cabañas, M.-J.; Baerlocher, C.; *J. Phys. Chem. B* **1998**, *102*, 44. [Crossref]
44. Mihályi, R. M.; Kollár, M.; Király, P.; Karoly, Z.; Mavrodinova, V.; *Appl. Catal., A* **2012**, *417-418*, 76. [Crossref]
45. Min, H.-K.; Park, M. B.; Hong, S. B.; *J. Catal.* **2010**, *271*, 186. [Crossref]
46. Ren, X.; Liang, J.; Wang, J.; *J. Porous Mater.* **2006**, *13*, 353. [Crossref]
47. Blasco, T.; Corma, A.; Martínez-Triguero, J.; *J. Catal.* **2006**, *237*, 267. [Crossref]
48. Zhao, G.; Teng, J.; Xie, Z.; Jin, W.; Yang, W.; Chen, Q.; Tang, Y.; *J. Catal.* **2007**, *248*, 29. [Crossref]
49. Védryne, J. C.; Auroux, A.; Bolis, V.; Dejaifve, P.; Naccache, C.; Wierzchowski, P.; Derouane, E. G.; Nagy, J. B.; Gilson, J. P.; van Hooff, J. H. C.; van den Berg, J. P.; Wolthuizen, J.; *J. Catal.* **1979**, *59*, 248. [Crossref]
50. Zheng, S.; Heydenrych, H. R.; Röger, H. P.; Jentys, A.; Lercher, J. A.; *Top. Catal.* **2003**, *22*, 101. [Crossref]
51. Muller, M.; Harvey, G.; Prins, R.; *Microporous Mesoporous Mater.* **2000**, *34*, 135. [Crossref]
52. Cheng, L.; Ye, X. P.; *Catal. Lett.* **2009**, *130*, 100. [Crossref]
53. Schenkel, R.; Jentys, A.; Parker, S. F.; Lercher, J. A.; *J. Phys. Chem. B* **2004**, *108*, 15013. [Crossref]
54. Kondo, J. N.; Ito, K.; Yoda, E.; Wakabayashi, F.; Domen, K.; *J. Phys. Chem. B* **2005**, *109*, 10969. [Crossref]
55. Natal-Santiago, M.; Dumesic, J.; *J. Catal.* **1998**, *175*, 252. [Crossref]
56. Wang, X.; Wan, F.; Gao, Y.; Liu, J.; Jiang, K.; *J. Cryst. Growth* **2008**, *310*, 2569. [Crossref]
57. Karge, H. G.; Boldingh, E.; *Catal. Today* **1988**, *3*, 379. [Crossref]
58. Cerqueira, H. S.; Ayrault, P.; Datka, J.; Guisnet, M.; *Microporous Mesoporous Mater.* **2000**, *38*, 197. [Crossref]
59. Karge, H. G.; *Stud. Surf. Sci. Catal.* **2001**, *137*, 707. [Crossref]

Submitted: September 20, 2022

Published online: March 3, 2023

